Journal of Alloys and Compounds 509 (2011) 9150–9156

Contents lists available at ScienceDirect

Journal of Alloys and Compounds

journal homepage: www.elsevier.com/locate/jallcom

Effect of surface nanocrystallization on the microstructural and corrosion characteristics of AZ91D magnesium alloy

M. Laleh, Farzad Kargar*

Department of Materials Engineering, Faculty of Engineering, Tarbiat Modares University, P.O. Box 14115-143, Tehran, Iran

ARTICLE INFO

Article history:
Received 19 February 2011
Received in revised form 21 June 2011
Accepted 22 June 2011
Available online 29 June 2011

Keywords:
Nanostructured layer
AZ91D magnesium alloy
SMAT
Grain refinement
Corrosion

ABSTRACT

Surface distinct deformed layers with thicknesses up to 150 μm, with grain size in the top most surface is in the nanometer scale, were produced on AZ91D magnesium alloy using surface mechanical attrition treatment (SMAT). Effects of different ball size on the properties of the SMATed samples were investigated. The microstructural, grain size, hardness and roughness features of the treated surfaces were characterized using optical microscopy (OM), scanning electron microscopy (SEM), X-ray diffraction (XRD), micro-indenter and digital roughness meter, respectively. Corrosion behavior of the samples was evaluated using potentiodynamic polarization and electrochemical impedance spectroscopy (EIS) techniques. It is found that the ball diameter does not have a significant effect on the top surface grain size, but the thickness of the deformed layer increases with increase of ball size, from 50 μm for 2 mm balls to 150 μm for 5 mm balls. For all of the SMATed samples, the top surface microhardness value increased significantly and did not show any obvious change for samples treated with different balls. Corrosion studies show that the corrosion resistance of the sample treated with 2 mm balls is higher than that of those treated with 3 mm and 5 mm balls. This can be mainly attributed to the surface roughness and defects density of the samples, which are higher for the SMATed samples with 3 mm and 5 mm balls compared with that of sample SMATed with 2 mm balls.

1. Introduction

Magnesium can be considered as an "ultra light weight" metal, because it has one quarter of the density of steel and only two-third that of aluminum and a high strength to weight ratio relative to either of steel and aluminum. These advantages have made magnesium and its alloys attractive in a wide range of industrial applications where structures with light weight and high strength are required, such as aerospace and automobile applications. However, magnesium alloys exhibit poor wear and low corrosion resistance that seriously limit their potential use in industrial practice [1–4]. In most cases, the failures of materials such as wear, corrosion and fatigue occur on the surface. On the other hand, these failures are very sensitive to the microstructure and properties of the materials surface [5,6]. Hence, optimization of the surface microstructure and properties of the materials can be an effective approach to improve their properties and service lifetime. It has been also verified that the surface microstructural refinement induced by different plastic deformation methods is an effective way for surface modification of bulk materials [7–9]. So far, various techniques based on severe plastic deformation have been developed for grain refinement in metals and alloys in order to enhance their physical and chemical properties, such as cold-rolling (CR) [10], equal channel angular pressing (ECAP) [11], high pressure torsion (HPT) [12], high energy shot peening (HESP) [13] and surface mechanical attrition treatment (SMAT) [14–21]. Among them, CR, ECAP and HPT have been usually used for synthesizing ultrafine-grained materials for which grain size of the final refined structure, in most of these cases, is in the micrometer or submicrometer range. But grain size of the metals and alloys can be refined down to nanoscale by using SMAT. This method can induce grain refinement into the nanometer regime in the surface of the bulk materials via generation of high plastic strain. Experimental investigations have shown that the mechanism of the grain refinement and refining process are strongly dependent on the structure of the materials (e.g. body-centered cubic (BCC), face-centered cubic (FCC) and hexagonal close packed (HCP)) and intrinsic properties (e.g. stacking fault energy (SFE)) of the materials [16,22]. Furthermore, the SMAT parameters such as treatment time, vibrating frequency and ball diameter can affect the final surface properties [15,23,24]. The results of grain refinement demonstrate the SMAT process is an effective technique for surface nanocrystallization. The recent studies have usually concentrated on the SMAT effect on the hardness,

* Corresponding author. Tel.: +98 21 77513923; fax: +98 21 77513923.
E-mail addresses: laleh.m.1992@gmail.com (M. Laleh), farzad.kargar@gmail.com (F. Kargar).

0925-8388/$ – see front matter © 2011 Elsevier B.V. All rights reserved.
doi:10.1016/j.jallcom.2011.06.094

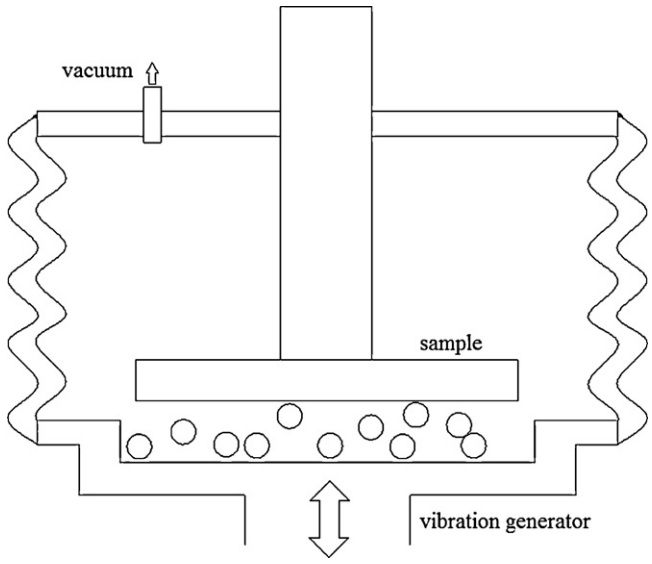

Fig. 1. Schematic of the surface mechanical attrition treatment set up.

wear, tensile and bending strength, thermal stability and fatigue life of the materials. However, the effect of SMAT on the corrosion properties of the magnesium alloys has rarely been investigated. On the other hand, the effect of ball diameter on the final properties of the nanocrystalline surface layer is still lacking. So, in the present work, AZ91D magnesium alloy with high performance was chosen for SMAT process in order to investigate the effect of ball size on the properties of the deformed layer.

2. Experimental details

2.1. A description of SMAT process

The SMAT process is a technique for surface nanocrystallization of metals and alloys. System includes a vacuum chamber (made of stainless steel), vibrating machine (with a vibrating frequency of 20 kHz) and stainless steel balls. The schematic illustration of the SMAT set-up is shown in Fig. 1. As mentioned previously, the main influencing parameters of SMAT are vibrating frequency, treatment time and ball diameter. The sample surface was impacted by multidirectional and random peening of flying balls. Each impacting of balls to the surface will result in plastic deformation in the surface layer of the treated sample. As a consequence, repeated impacting at high strain rate onto the sample surface leads to severe plastic deformation in the surface layer. In this experiment the SMAT process was performed in vacuum at vibrating frequency of 20 kHz using stainless steel balls with different diameters (2, 3 and 5 mm) for 30 min.

2.2. Sample preparation and testing

The material used in this study was AZ91D magnesium alloy (with chemical composition of Al 8.5–9.5%, Zn 0.50–0.90%, Mn 0.17–0.27 and Mg balance) rod (25 mm diameter and 5 mm thickness). Prior to SMAT, the specimens were ground with SiC abrasive papers (up to 1200 grit) and then ultrasonically degreased in acetone. An optical microscope (Olympus BX51M) was used to observe the microstructural development along sections perpendicular to the treated surface of the samples. Before microstructural observation, the samples were mechanically polished using silicon carbide papers up to grade 1000, then on a polishing cloth with water based liquid suspension of 0.5 μm alumina, and finally etched in a solution consisting of 0.7 mL phosphoric acid, 5 g picric acid and 100 mL ethanol. The average grain size of the top surface layer of the SMATed samples was obtained from X-ray diffraction (XRD) line broadening. XRD experiments were performed on a Siemens D-500 diffractometer with Cu Kα radiation in the range of 30–80° with a step width of 0.02°. The Vickers microhardness (HV) tests on the cross-sections of the samples were carried out on a Buehler microtest device with an applied load of 25 g and a loading time of 15 s. The microhardness variation was measured along the depth (up to 400 μm from the top surface), and the distance between any two neighboring indentations was at least 10 μm. The average surface roughness (R_a) and peak-to-valley (PV) of the SMATed magnesium samples were measured using a stylus type surface profilometer (Taylor Hobson Surtronic 25) with an resolution of 0.01 μm. Corrosion tests were carried out using a potensiostat/galvanostat (EG&G Princeton Applied Research 273A) system. The three electrode cell with the SMATed samples as the working electrode, a platinum grid as the counter electrode and a saturated calomel electrode (SCE) as the reference electrode was used in the electrochemical experiments. All experiments were carried out in a 3.5 wt.% NaCl solution and the exposed area of the working electrode with the solution was 1 cm^2. After the electrochemical testing system became stable (about 10 min), the EIS tests were carried out by sweeping frequencies from 100 kHz to 10 mHz with an AC voltage amplitude of 10 mV. The potentiodynamic polarization curves were obtained at a scan rate of 1 mV/S from −200 mV to 1000 mV versus open circuit potential. Each electrochemical test was repeated three times in order to assure its reproducibility.

3. Results and discussion

3.1. Microstructure

The cross-sectional microstructure observations of the SMATed samples by OM are shown in Fig. 2. It can be clearly seen that the microstructure morphology of the deformed layers differ obviously from that the substrate, and the thickness of the distinct deformed layer increases with increase in the ball diameter (from about 50 μm for SMATed sample with 2 mm balls to about 150 μm for SMATed sample with 5 mm balls). Grain boundaries and β-phase ($Mg_{17}Al_{12}$) cannot be identified in OM observations of the deformed layer compared to the matrix, indicating that the grains in the treated layer are significantly refined in comparison to that in the coarse-grained matrix. High density of deformation twins can be found in the depth about 50–200 μm from the top surface. XRD patterns of the AZ91D magnesium alloy before and after SMAT are shown in Fig. 3. As can be seen, after SMAT the diffraction intensity decreased greatly and the diffraction lines broadened which can be mainly attributed to the grain refinement and lattice distortion. In addition, the peaks of β-phase disappeared in the XRD patterns of the SMATed samples. This fact indicates that the β-phases are resolutionised in the magnesium matrix [25]. The slight shift in diffraction angle for treated sample with 5 mm balls can be due to the increase in crystalline imperfections/defects induced during SMAT. The average grain size of the treated samples was calculated according to the Williamson–Hall method (Eq. (1)) [26].

$$B\cos\ \theta = \frac{k\lambda}{l} + \eta \sin\theta \quad (1)$$

where B is full-width-half-max of the peak ($B_{size} + B_{strain}$), θ is the diffraction angle, k is constant (0.9), λ is the wavelength of the X-ray (1.54 nm), l is the grain size and η is the micro strain. Variation of the average grain size of the top surface layer and the thickness of the deformed layers with the ball diameter are shown in Fig. 4. Although the mean grain size of the SMATed samples is nearly the same, the thickness of the deformed layer is very different, and is a function of the ball size.

3.2. Microhardness

Fig. 5 shows the variation of microhardness with distance from the SMATed surface to the substrate for different samples. The thickness of the total deformed layer generated by SMAT in AZ91D magnesium alloy samples can be identified from Fig. 5, which is in good agreement with OM observations shown in Figs. 2 and 4. Furthermore, it can be seen that the microhardness of the top-most layer of the SMATed samples is at least twice in comparison with the hardness of the substrate. It is important to note that the deformed layer has a gradient structure which is identified from Figs. 2 and 5, i.e. the microhardness of the SMATed sample gradually decreases and approaches the value for the core material. According to the well-known Hall-Petch relationship, the increase of the surface hardness of the SMATed samples can be attributed to the both effects of the grain refinement and work-hardening. The grain size strengthening effect in AZ91D magnesium alloy (with HCP crystal structure) is high relative to other metals with BCC and FCC crystal

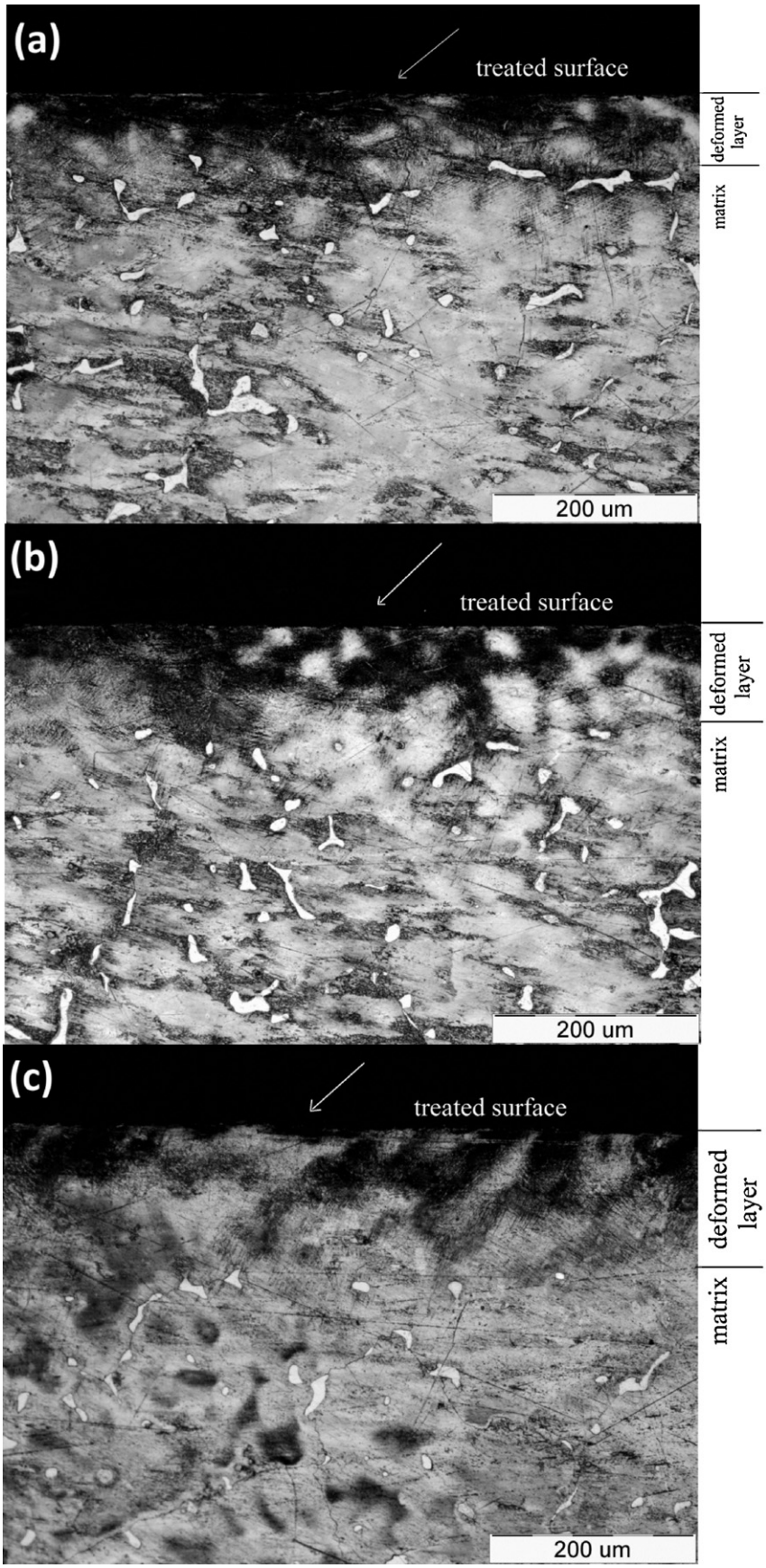

Fig. 2. Cross-sectional OM observations of the SMATed AZ91D magnesium alloy with (a) 2 mm, (b) 3 mm and (c) 5 mm balls treated/SMATed for 30 min.

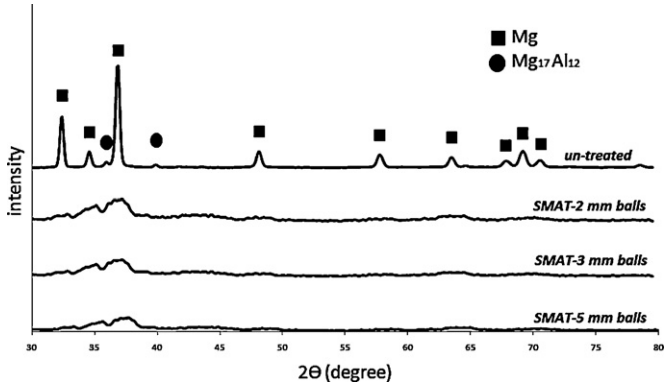

Fig. 3. XRD patterns of the as-received and different SMATed samples.

structure, because Mg has a large Taylor factor [6,27]. Furthermore, re-dissolution of the β-phase due to the high strain induced during SMAT can be considered as another reason for microhardness increase [6]. On one hand, the OM observations (Fig. 2) do not show any β-phase in the treated layer; additionally the main peaks of the β-phase in the XRD patterns (Fig. 3) disappeared for all of the SMATed samples. When the sample was subjected to the SMAT, the Gibbs free energy of the sample increased as a result of the increase in both of the grain boundary surface area and distortion. So, from the thermodynamic point of view, this sample tends to decrease its Gibbs free energy by any event such as re-dissolution of the β-phase. Besides, the use of balls with a larger size in the SMAT increases surface hardness. It is verified that in the constant conditions (vibration frequency, materials of the balls), the larger balls in the SMAT delivers a greater impact load and accordingly yields a higher surface microhardness than the smaller balls.

3.3. Roughness

There are a wide range of numerical parameters and measurement methods available for characterization of surface roughness. However, height-based parameters are commonly used in basic roughness characterizations because they can easily be determined from stylus type profilometer. The arithmetic mean roughness (R_a value) is defined as the average of the absolute value of all area values, $z(x)$, contained within a profile length (l); according to Eq. (2).

$$R_a = \frac{1}{l}\int_0^l |Z(x)|dx \quad (2)$$

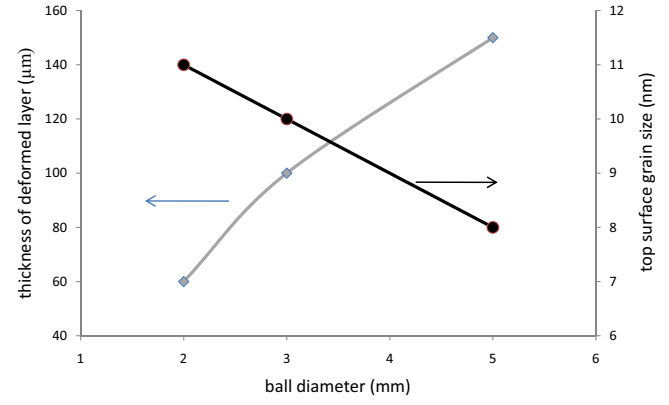

Fig. 4. Variation of deformed layers thickness and the top surface grain size of the SMATed samples as a function of ball size measured from microscopic observations and XRD patterns, respectively.

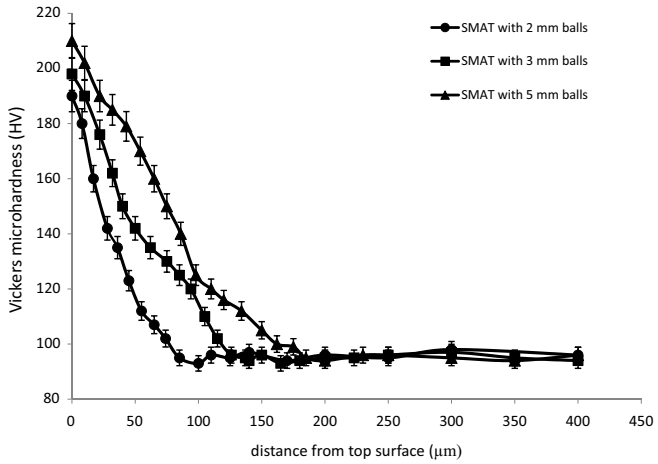

Fig. 5. Variation of the Vickers microhardness along depth perpendicular to the treated direction for the different SMATed samples.

Another parameter used for roughness measurements is the vertical distance between the highest peak and the lowest valley (PV) of the profile. The R_a and PV values were used in this study because they have been used routinely in industrial applications to quantify the changes in the surface morphology, and they are reasonable representatives of the roughening behavior of the materials. The changes of R_a and PV of the SMATed samples as a function of ball size are shown in Fig. 6. Note that the data points shown in these curves are the average values of three traces. Both curves indicate that the ball diameter has an appreciable effect on the roughening behavior of the SMATed samples. As can be clearly seen from both curves, the amounts of PV and R_a values were increased with increasing of the ball diameter. Present results about the effect of the ball diameter on the surface roughness are in good agreement with the investigations performed on the Al 5052, which previously shown that the maximum PV value was increased from 65 to 110 μm with increasing of ball diameter from 5 to 7.9 mm [28,29].

3.4. Corrosion behavior

The corrosion behavior of the as-received and SMATed samples was studied by potentiodynamic polarization and electrochemical impedance spectroscopy (EIS). The potentiodynamic curves as a function of ball diameter during immersion in 3.5 wt.% NaCl solution at room temperature are shown in Fig. 7. Values of corrosion current density (i_{corr}) and corrosion potential (E_{corr}) of the as-received and SMATed samples, which are derived from polarization

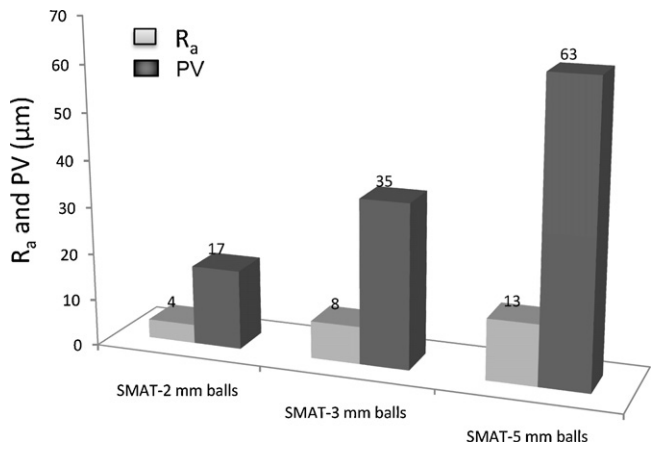

Fig. 6. Variation of R_a and PV of the SMATed samples as a function of ball size.

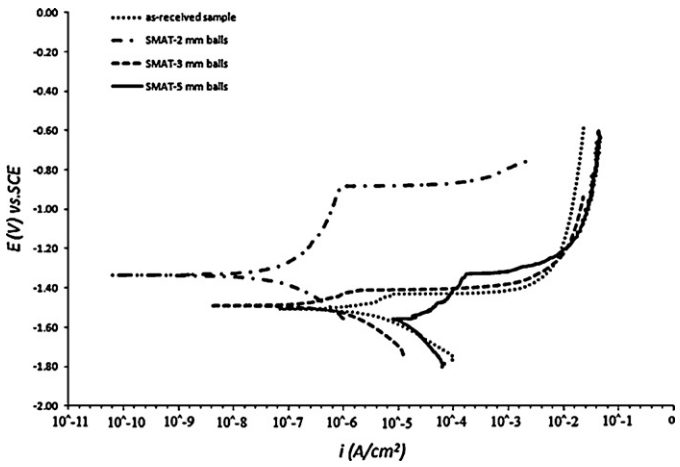

Fig. 7. Potentiodynamic polarization curves of the as-received and different SMATed samples recorded in 3.5 wt.% NaCl solution.

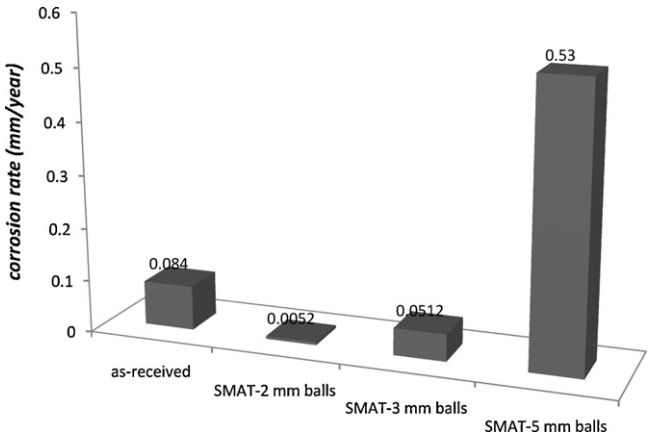

Fig. 8. Corrosion rates of the as-received and different SMATed samples in 3.5 wt.% NaCl solution measured by Eq. (3).

curves, are summarized in Table 1. Sample treated with 2 mm balls shows an obvious anodic shift at E_{corr} and a significant decrease of i_{corr} but, the SMATed sample with 5 mm balls shows opposite trend. Although, the changes in E_{corr} and i_{corr} for the SMATed sample with 3 mm balls are not significant, the treated sample with 5 mm balls shows a relatively obvious change in E_{corr} (52 mV shift in active direction) and a dramatic increase of i_{corr} (about one order of magnitude) compared with to the as-received one. Corrosion rate of the samples can be calculated by Eq. (3).

$$\text{Corrosion rate}\left(\frac{mm}{y}\right) = \frac{3.28M}{n\rho} i_{corr} \quad (3)$$

where, M is the atomic mass, n is the number of electrons freed by the corrosion reaction and ρ is the alloy density. The corrosion rate for the as-received and SMATed samples are presented in Fig. 8. As can be seen, the corrosion rate of the treated sample with 2 mm balls is the lowest value compared with other samples. Nyquist diagrams obtained from EIS tests for as-received and SMATed magnesium alloy specimens are shown in Fig. 9. All of the samples showed a capacitive arc at high and intermediate frequencies, which can be attributed to the metal dissolution during the corrosion process. The diameter of these arcs is associated with the charge transfer resistance, i.e. the corrosion resistance [30–33]. The diameter of the capacitive arc of the SMATed sample with 5 mm balls is much smaller than that of as-received and other SMATed samples, i.e. it has the weakest corrosion resistance. The surface morphologies of the SMATed samples after polarization test in 3.5 wt.% NaCl solution are also shown in Fig. 10. As can be seen, the extent of corrosive attack for samples SMATed using 2 and 3 mm balls is relatively less while the sample treated using 5 mm balls exhibits severe corrosive attack. The corrosion behavior of the materials depends on many factors. In the case of the SMATed sample, structural change at the surface layer, i.e. grain refinement into nano-scale regime and surface roughness, play important roles in its corrosion resistance [23]. Besides, the surface roughness has a greater effect on the corrosion resistance. From the corrosion point of view, a smoother surface offers a better corrosion resistance and vice versa [1,34]. As previously explained in Section 3.3, SMAT caused an increase in surface roughness and the extent of roughness increased with ball size (Fig. 6). It has also been reported that the increase in the surface roughness would lead to an increase in the corrosion rate [35,36]. Although the increase in surface roughness in the SMATed sample using 5 mm balls cause a decrease in corrosion resistance (increase in corrosion rate), the sample treated using 2 mm balls offer better corrosion resistance than the untreated sample. Polarization curve obtained for this sample reveal the formation of a passive film as shown in Fig. 7. The enhanced surface passivity observed for the SMATed sample with 2 mm balls can be probably attributed to the surface nanocrystallization. Grain refinement is another important factor in determining the corrosion behavior as well as the surface roughness [33,37]. According to the previous investigations, the grain size has a dual effect on the corrosion resistance of the materials. On one hand, it has been reported that the decrease in the grain size can cause an increase in corrosion rate [33,37] and on the other hand some literatures have shown an improvement in corrosion resistance with a decrease in grain size [38–40]. So, the corrosion characteristic of the SMATed samples cannot be examined just in term of the grain size, and other parameters such as extent of deformation, imperfections/defect density and micro strain should be considered. Investigations have shown that the cold deformation up to a certain percent can lead to an improvement in corrosion resistance of the materials. For

Table 1
Corrosion potential (E_{corr}) and corrosion current density (i_{corr}) of the samples in 3.5 wt.% NaCl solution.

Sample	E vs. SCE	i_{corr} (μA/cm²)
As-received	−1.509	3.906
SMAT-2 mm balls	−1.334	0.243
SMAT-3 mm balls	−1.489	2.395
SMAT-5 mm balls	−1.561	24.83

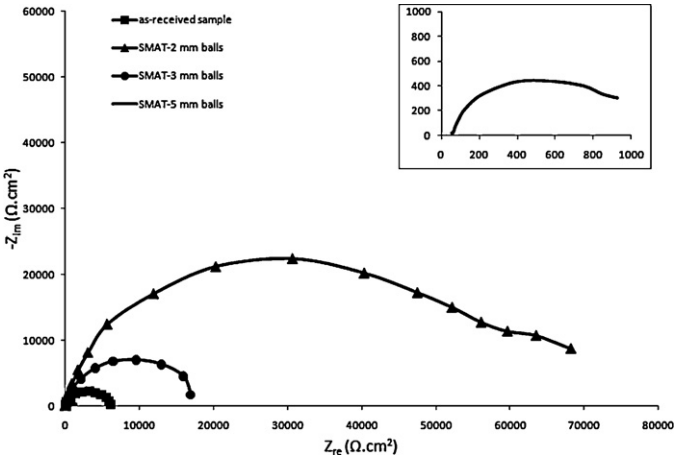

Fig. 9. Nyquist plots of impedance spectra of the as-received and SMATed AZ91D Mg alloy in 3.5 wt.% NaCl solution. Inset is the high magnification of impedance spectra of the SMATed sample with 5 mm balls.

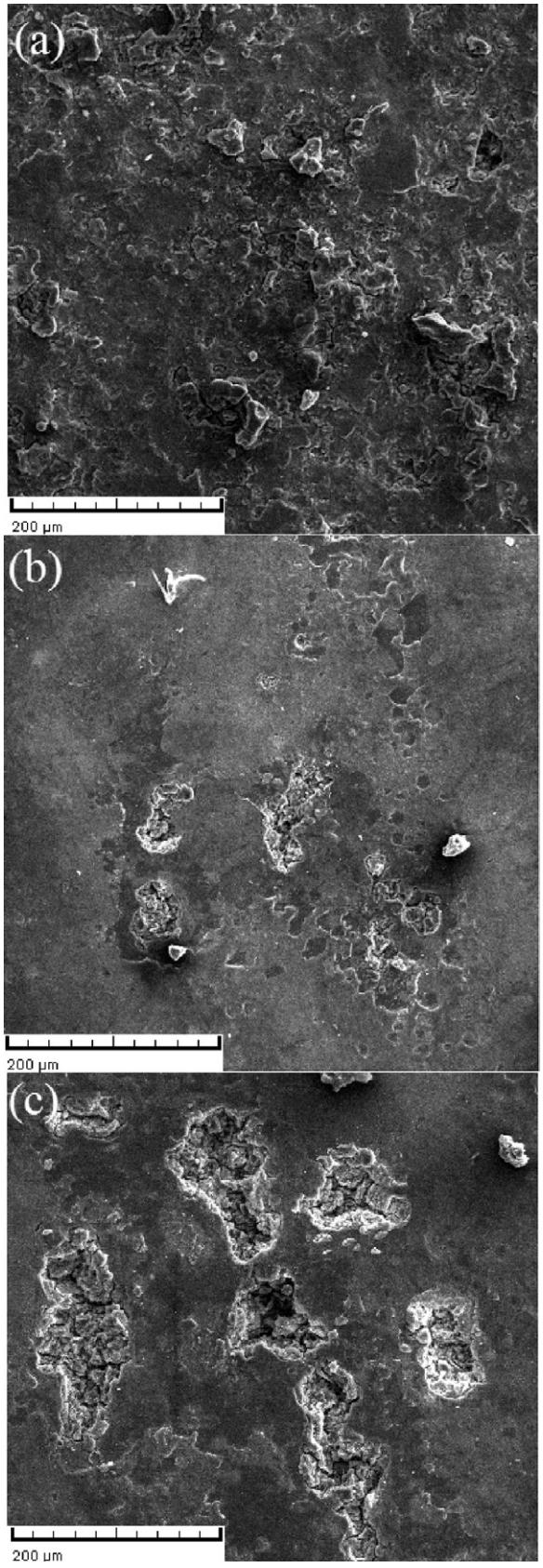

Fig. 10. Surface morphologies of SMATed magnesium alloy samples after polarization from −250 to +250 mV (SCE) from their respective OCPs in 3.5 wt.% NaCl solution: (a) SMATed using 2 mm balls; (b) SMATed using 3 mm balls; and (c) SMATed using 5 mm balls.

example, conventional extrusion of AZ31 magnesium alloy (with an extrusion ratio of 91.34%) has resulted in an enhancement in corrosion resistance, but a further increase in the extent of the extrusion ratio (98.99%) causes to decrease in the corrosion resistance [41]. The increase in the dislocations density due to the cold deformation would create a large number of active sites and as a result promote the rate of the corrosion phenomenon. It is well known that the SMAT can induce an extremely high free energy state and dislocation density in the near-surface region of the material [23,40]. It appears that the ball size in the SMAT plays an important role in formation of dislocations, and with an increase in the ball size the defects and dislocations density in the SMATed surface increase. As previously mentioned, XRD patterns (Fig. 3) demonstrate the relatively high distortion in the SMATed sample treated using 5 mm balls. So, the increase in both the surface roughness and dislocations/defects density in the sample treated using 5 mm balls causes a decrease in corrosion resistance despite of the decrease in the grain size. In addition to the mentioned factors, the effect of dissolution of β-$Mg_{17}Al_{12}$ after SMAT on the final corrosion resistance also should be considered. It has been shown that the corrosion resistance of the AZ91D alloy may be enhanced by dissolution of the β-$Mg_{17}Al_{12}$ phase [42–44]. On one hand, presence of β-$Mg_{17}Al_{12}$ leads to galvanic coupling with α-Mg and accelerates the corrosion process. On the other hand, the β-$Mg_{17}Al_{12}$ phase can act as a barrier against corrosion propagation. In view of these two opposite effects of β phase to corrosion resistance of AZ91D alloy, the corrosion resistance of the magnesium samples can be explained. In the case of the as-received sample, the β-phase acts as a galvanic cathode and accelerates the localized corrosion. But, resolutionised of the β-phase in the SMATed sample would lead to transform from localized corrosion to uniform corrosion. In this study, it seems that the dissolution of β-$Mg_{17}Al_{12}$ phase had a positive effect on the corrosion resistance.

4. Conclusions

Surface mechanical attrition treatment was used to induce plastic deformation and grain refinement in the AZ91D magnesium alloy. The effect of ball size on the properties of the treated samples was investigated. The depth of the plastically deformed layer was increased from about 50 μm for SMATed sample with 2 mm balls to about 150 μm for the treated sample with 5 mm balls. Grain refinement and microstrain resulted in the broadening of the XRD peaks. The slight decrease in the top surface grain size (from 11 to 8 nm) was observed with an increase in the ball diameter (from 2 to 5 mm). It is found that after SMAT, β-$Mg_{17}Al_{12}$ peaks were not apparent in the XRD patterns. The surface hardness of the SMATed samples was increased at least by a factor of two, which is mainly due to the grain refinement and dissolution of the β-$Mg_{17}Al_{12}$ phase. SMAT increased the surface roughness; increase in ball diameter increases the roughness. Electrochemical studies reveal that the corrosion resistance of the SMATed samples depends on increase in microstrain and defect density, grain refinement and dissolution of β-$Mg_{17}Al_{12}$ phase. Corrosion tests results showed that SMAT using 5 mm balls decreased the corrosion resistance because of the increase in the defect density during the treatment in spite of grain refinement. In contrast, SMAT using 2 mm balls increased the corrosion resistance significantly.

References

[1] M. Laleh, A. Sabour Rouhaghdam, T. Shahrabi, A. Shanghi, J. Alloys Compd. 496 (2010) 548–552.
[2] K. Xu, A. Wang, Y. Wang, X. Dong, X. Zhang, Z. Huang, Appl. Surf. Sci. 256 (2009) 619–626.
[3] D.Y. Hwang, Y.M. Kim, D.Y. Park, B. Yoo, D.H. Shin, Electrochim. Acta 54 (2009) 5479–5485.

[4] K. Mueller, S. Mueller, J. Mater. Process. Technol. 187–188 (2007) 775–779.
[5] L. Wang, Mater. Sci. Eng. A 263 (1999) 210–216.
[6] Y. Wei, B. Liu, L. Hou, B. Xu, G. Liu, J. Alloys Compd. 452 (2008) 336–342.
[7] Z.B. Wang, N.R. Tao, W.P. Tong, J. Lu, K. Lu, Acta Mater. 51 (2003) 4319–4329.
[8] N.R. Tao, Z.B. Wang, W.P. Tong, M.L. Sui, J. Lu, K. Lu, Acta Mater. 50 (2002) 4603–4616.
[9] W. Li, P. Liu, F. Ma, X. Liu, Y. Rong, J. Alloys Compd. 509 (2011) 518–522.
[10] M.R. Barnett, M.D. Nave, C.J. Bettles, Mater. Sci. Eng. A 386 (2004) 205–211.
[11] R.Z. Valiev, J. Mater. Sci. 42 (2007) 1483–1490.
[12] K. Massaki, Z.J. Horita, G. Terence, Mater. Sci. Eng. A 488 (2008) 117–124.
[13] L.F. Hou, Y.H. Wei, B.S. Liu, B.S. Xu, Trans. Nonferrous Met. Soc. China 18 (2008) 1053–1057.
[14] A. Revesz, P. Szommer, P.J. Szabo, L.K. Varga, J. Alloys Compd. 509S (2011) S482–S485.
[15] A. Revesz, L. Takacs, J. Alloys Compd. 441 (2007) 111–114.
[16] K. Lu, J. Lu, Mater. Sci. Eng. A 375–377 (2004) 38–45.
[17] H.W. Zhang, Z.K. Hei, G. Liu, J. Lu, K. Lu, Acta Mater. 51 (2003) 1871–1881.
[18] C. Wen, W. Li, Y. Rong, Mater. Sci. Eng. A 481–482 (2008) 484–488.
[19] W. Li, W. Xu, X. Wang, Y. Rong, J. Alloys Compd. 474 (2009) 546–550.
[20] M. Laleh, F. Kargar, Mater. Lett. 65 (2011) 2295–2298.
[21] M. Laleh, F. Kargar, Mater. Lett. 65 (2011) 1935–1937.
[22] N.R. Tao, K. Lu, Scripta Mater. 60 (2009) 1039–1043.
[23] T. Balusamy, S. Kumar, T.S.N. Sankara Narayanan, Corros. Sci. 52 (2010) 3826–3834.
[24] B. Arifvianto, M. Mahardika Suyitno, P. Dewo, P.T. Iswanto, U.A. Salim, Mater. Chem. Phys. 125 (2011) 418–426.
[25] L.F. Hou, Y.H. Wei, X.F. Shu, B.S. Xu, J. Alloys Compd. 492 (2010) 347–350.
[26] G.K. Williamson, W. Hall, Acta Metall. 1 (1953) 22–31.
[27] W.J. Kim, H.G. Jeong, H.T. Jeong, Scripta Mater. 61 (2009) 1040–1043.
[28] K. Dai, J. Villegas, Z. Stone, L. Shaw, Acta Mater. 52 (2004) 5771–5782.
[29] K. Dai, J. Villegas, L. Shaw, Scripta Mater. 52 (2005) 259–263.
[30] N. Pebere, C. Riera, F. Dabosi, Electrochim. Acta 35 (1990) 555–561.
[31] C. Cao, Electrochim. Acta 35 (1990) 831–836.
[32] C. Cao, Electrochim. Acta 35 (1990) 837–844.
[33] D. Song, A.B. Ma, J.H. Jiang, P.H. Lin, D.H. Yang, J.F. Fan, Corros. Sci. 53 (2011) 362–373.
[34] W. Li, D.Y. Li, Acta Mater. 54 (2006) 445–452.
[35] E. Arslan, Y. Totic, E. Demirci, A. Alsaran, J. Mater. Eng. Perform. 19 (2010) 428–433.
[36] D.Y. Hwang, B.Y. Yoo, J.Y. Cho, D.H. Lee, D.H. Shin, Electrochim. Acta 54 (2009) 5479–5485.
[37] K-d. Xu, J-n. Wang, A-h. Wang, H. Yan, X-l. Zhang, Z-w. Huang, Curr. Appl. Phys. 11 (2011) 677–681.
[38] N.N. Aung, W. Zhou, Corros. Sci. 52 (2010) 589–594.
[39] N. Birbilis, K.D. Ralston, S. Virtanen, H.L. Fraser, C.H.J. Davies, Corros. Eng. Sci. Technol. 45 (2010) 224–230.
[40] C. op't Hoog, N. Biribilis, Y. Estrin, Adv. Eng. Mater. 10 (2008) 579–582.
[41] G. Ben Hamu, D. Eliezer, L. Wagner, J. Alloys Compd. 468 (2009) 222–229.
[42] W. Zhou, T. Shen, N. Naing Aung, Corros. Sci. 52 (2010) 1035–1041.
[43] M.C. Zhao, M. Liu, G.L. Song, A. Atrens, Corros. Sci. 50 (2008) 1939–1953.
[44] G.L. Song, A.L. Bowles, D.H. StJohn, Mater. Sci. Eng. A 366 (2004) 74–86.